Structural Studies of *Impatiens balsamina* Antimicrobial Protein (Ib-AMP1)†

Sunil U. Patel,*,‡ Rupert Osborn,§ Sarah Rees,§ and Janet M. Thornton*,‡

Biomolecular Structure and Modelling Unit, Department of Biochemistry and Molecular Biology, University College London, Gower Street, London WC1E 6BT, U.K., and Zeneca Agrochemical, Jealott's Hill Research Station, Bracknell, Berkshire RG42 6ET, U.K.

Received July 17, 1997; Revised Manuscript Received October 22, 1997⊗

ABSTRACT: Structural studies of Ib-AMP1, a small antimicrobial peptide derived from the seeds of *Impatiens balsamina* have been performed using circular dichroism (CD) and two-dimensional proton nuclear magnetic resonance (^{1}H NMR). This 20-residue peptide is highly basic with five arginine residues and contains four cysteines which form two intramolecular disulfide bonds. CD results reveal that the peptide may include a β-turn but do not show evidence for either helical or β-sheet structure over a range of temperature and pH. Structural information from NMR was obtained in the form of proton−proton internuclear distances inferred from NOEs and dihedral angle restraints from spin−spin coupling constants, which were used for distance geometry calculations. Owing to the difficulty in obtaining the correct disulfide connectivities by chemical methods, three separate calculations were performed; with no disulfides and with the two possible alternate disulfide connectivities. Results from distance geometry calculations reveal that although the peptide is small, the cysteines constrain part of it to adopt a well-defined main chain conformation. From residue 6 to 20, the backbone is well defined, whilst the N-terminal region, residues 1−5, has very few constraints and appears to be very flexible. In the defined core region, there are three β-turns at residues 9−12, 10−13, and 12−15. The side chains show no strong interactions in the NMR spectra and are therefore thought to adopt multiple conformations. Superposition of the structures generated shows that the peptide has two hydrophilic patches which are at opposite ends of the molecule separated by a large hydrophobic patch. Little is known about the mode of action of this protein, but it is thought to interact with a membrane-bound receptor, and possible sites of interaction are discussed. The structures determined are compared with those of the α-conotoxins, which are also highly basic proteins with similar disulfide connectivities.

Plants have been shown to produce a wide range of antifungal and antimicrobial proteins. These include the chitinases, glucanases, lipid transfer proteins, chitin binding lectins, and thionins (*1*−*14*). While the true physiological function of these proteins is not fully understood, it is thought that they play an important role in the plant's defense against microbial infections. Ib-AMP1 is one of a novel family of four highly homologous peptides found in the seeds of *Impatiens balsamina* (Figure 1) (*15*). This family of peptides is the smallest of the antimicrobial peptides isolated to date from plants.

The goal of this work has been to determine the structure of Ib-AMP1 and to use this information to gain better understanding of structure/function relationships and to form a basis for agrochemical design or for genetic engineering of fungal resistance in transgenic plants. Circular dichroism (CD)[1] was performed to determine the secondary structure of the peptide and its temperature and pH stability. 2D ^{1}H NMR was used to determine the geometric restraints from which the three-dimensional structure was derived.

MATERIALS AND METHODS

Biochemical Characterization. Purification, Mass Spectrometry, Circular Dichroism, and Binding Assay. Ib-AMP1 used in these studies was purified from *I. Balsamina* seeds as described previously (*15*). The protein was extracted from 1 kg of ground seeds, and following ammonium sulfate precipitation and dialysis, the basic protein fraction (PI > 9) was fractionated by cation-exchange chromatography. The peak of antifungal activity which corresponds to Ib-AMP1 was further fractionated by reverse-phase HPLC to yield a single well-resolved peak of absorbance at 210 nm. Protein purity and primary structure were determined using a high-resolution two reverse-geometry double-focusing mass spectrometer (VG ZAB-SE).

CD experiments were performed using a Jasco 600 spectropolarimeter to determine the secondary structure information, concentration and temperature effects, and pH stability of Ib-AMP1. The spectropolarimeter was calibrated with a freshly made aqueous solution of (+)−10-camphorsulfonic acid whose concentration was measured by absorbency at 285 nm. The samples were made in distilled water

† This work was supported in part by AIR Grant AIR2-CT94-1356 of the Commission of European Union.

* Corresponding authors: Fax, 0171-380-7193.
‡ University College London.
§ Jealott's Hill Research Station.

⊗ Abstract published in *Advance ACS Abstracts,* December 15, 1997.

[1] Abbreviations: CD, circular dichroism; NMR, nuclear magnetic resonance; DQF-COSY, double-quantum-filtered correlation spectroscopy; TOCSY, total correlation spectroscopy; NOESY, nuclear Overhauser effect spectroscopy.

S0006-2960(97)01747-9 CCC: $15.00
Published on Web 01/06/1998

```
                1   5     10    15   20
Ib-AMP1         QWGRRCCGWGPGRRYCVRWC
Ib-AMP2         QYGRRCCNWGPGRRYCKRWC
Ib-AMP3         QYRHRCCAWGPGRKYCKRWC
Ib-AMP4         QWGRRCCGWGPGRRYCRRWC

CONSENSUS       Q  #RCC WGPGR#YC#RWC
IDENTITY        *   *** ***** ** ***

G1              --ECC-NPACGRHYS--C--
GIA             --ECC-NPACGRHYS--CGK
GII             --ECC-HPACGKHFS--C--
SI              --ICC-NPACGPKYS--C--
SIA             --YCC-HPACGKNFD--C--
SII             -GCCC-NPACGKNYS--C--
MI              -GRCC-HPACGKNYS--C--
MII             -G-CC-SPVCHEH-SNLC--
PnIA            -G-CCSLPPCAANNPDYC--
PnIB            -G-CCSLPPCALSNPDYC--
EI              RDOCCYHPTCNMSNPQIC--
IMI             -G-CCSDPRCAWR----C--

CONSENSUS         CC  P C       C
IDENTITY          **  * *       *
```

FIGURE 1: Sequence alignment of *I. balsmina* antimicrobial peptides (Ib-AMP1−4) and α-conotoxins from various *Conidae*: GI, GIA, and GII from *C. geographus*, SI, SIA, and SII from *C. striatus*, MI and MII from *C. magus*, PnIA and PnIB from *C. pennaceusc*, EI from *C. ermineus*, and IMI from *C. imperialis*. The letter O represents hydroxyproline. The line "consensus" highlights the conserved pattern found within the *I. balsmina* and α-conotoxins, where an "★" denotes conserved identity and a "#" represents similarity. Highlighted in bold are amino acid similarities in the *I. balsmina* and α-conotoxin GI, GIA, and GII and the overall amino acid conservation.

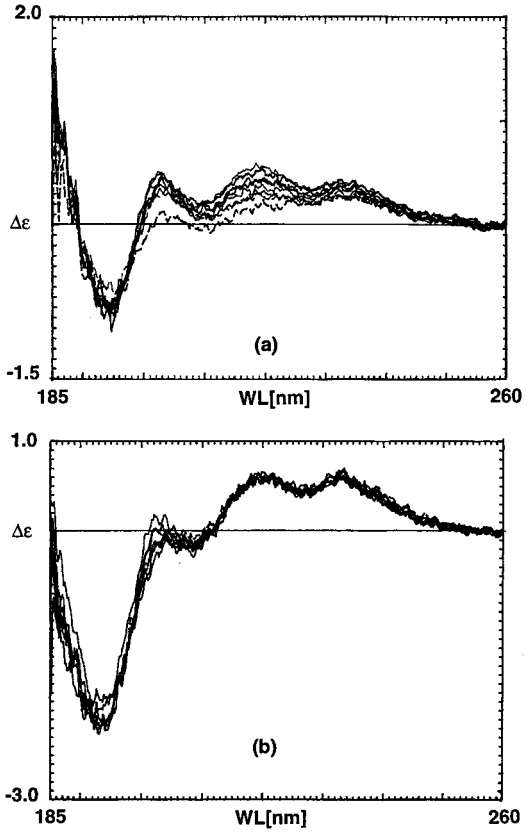

FIGURE 2: Circular dichroism spectra of Ib-AMP1. Panel a shows the effects of temperature from 19 to 90 °C. Panel b shows the effects of changes in pH from 4 to 10.

(0.5 mg/mL) and the pH adjusted with microliter additions of hydrochloric acid (0.1 M) or sodium hydroxide (0.1M). For temperature studies, the samples were made up in phosphate buffer at pH 7.00. The spectra were acquired in a single scan mode (10 nm/min) for each of the measurements in the UV region of 340−240 nm and 265−185 nm using demountable cuvettes of 1 and 0.02 cm optical path lengths. The data were baseline corrected.

Binding assays to investigate whether Ib-AMP1 binds to the acetylcholine receptor were carried out using an α-bungarotoxin binding assay. Binding of ^{3}H- labeled α-bungarotoxin (Amersham, U.K.) to blowfly (*Lucilia*) head membranes was carried out in a solution containing 50 mM Tris, pH 7.4, 120 nM NaCl, and 0.1 mM EDTA. Incubations were carried out at room temperature for 1 h. Ib-AMP1 was preincubated with the receptor preparation for $^1/_2$ h prior to addition of labeled toxin. Filtration was used to separate the membrane bound fraction prior to counting in a β-plate counter.

NMR Studies. NMR experiments were performed on Ib-AMP1 (0.6 mL, 2 mM) at a nonadjusted pH* 4.0, at 30 °C or 10 °C in either 100% D_2O or 90% H_2O/10% D_2O. Experiments were performed on Bruker AMX Varian Unity Plus 600 and 500 MHz spectrometers. In preliminary single-pulse experiments, a trace of dioxane was added as an internal reference and referenced at 3.765 ppm (at 30 °C) relative to TMS. DQF-COSY (*16*), TOCSY (*17, 18*), and NOESY (*19, 20*) experiments were performed with different spin-lock and mixing times. TOCSY spectra were recorded using a spin-lock field of ca. 8 kHz produced by an MLEV-17 pulse sequence (*21*). NOESY spectra with NOE mixing times of 100, 200, and 350 ms were recorded. To overcome the effects of dynamic range associated with the water peak, a pulse field gradient in the "watergate" sequence (*22*) was used in conjunction with the TOCSY and NOESY experiments. All 2D ^{1}H NMR experiments were performed in phase-sensitive mode (*23*). The 2D ^{1}H NMR experiments were usually recorded over a period of 20−40 h, typically acquiring 256 or 512 t_1 increments, with 16−80 scans per increment and either 4096 or 8192 data points per scan. The spectra were acquired with a spectral width of 8 kHz in F_1 and F_2 dimensions. Data processing was performed on a Sun Sparc 10 workstation using the Varian VNMR software (*24*). The original data were zero-filled to 1024 or 2048 complex points in F_1, and a shifted Gaussian window function was applied prior to Fourier transformation. A 1D Watergate ^{1}H NMR spectrum in H_2O was also acquired with 80 scans and 64K data points.

NMR Resonance Assignments. Spin systems were identified from the DQF-COSY and TOCSY spectra. Using TOCSY and NOESY spectra in water, arginine residues (five in total) were identified from the C_αH protons to C_ϵH protons and by reverse transfer pathway from the NH protons from the N_ϵH or C_ϵH protons to C_αH protons; glycine residues (four in total) were identified from the PH DQF-COSY/TOCSY spectra in water; valine was identified from the two methyl groups; the tryptophan and tyrosine residues (3 and 1, respectively) were identified from their NOE cross-peaks between the β protons belonging to the aromatic side chains to the δ protons of their aromatic rings; the proline residue was identified by the C_δH protons around 3.7 and 3.5 ppm coupling to the C_αH protons and by the NOE observed from the δ proton to the α protons of the preceding glycine. Furthermore, NOEs from the glycine C_αH protons to the C_δH

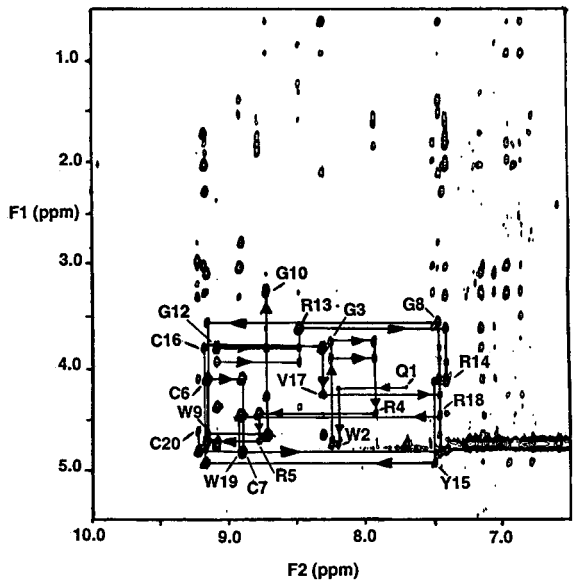

FIGURE 3: Fingerprint region from a NOESY spectrum of Ib-AMP1 recorded at 30 °C with a 200 ms mixing time. The sequential $d_{\alpha N}$ connectivities for residues 1−20 are indicated. Some cross-peaks for intraresidue NH−C_αH NOEs, though labeled, are not visible in this plot. These were observed at lower contour levels or in other spectra.

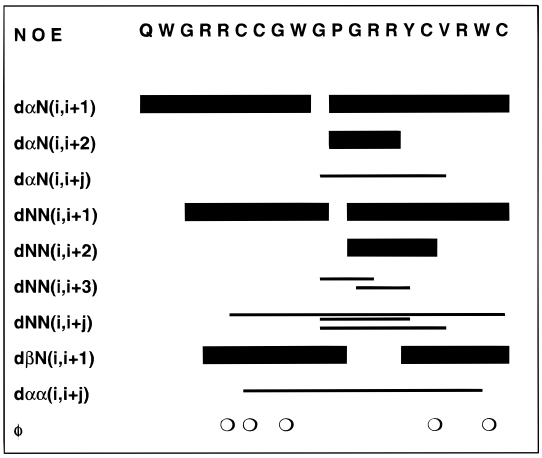

FIGURE 4: Summary of the sequential and medium-range NOEs identified for Ib-AMP1. $d_{\alpha N}(i,i+1)$, $d_{\alpha N}(i,i+2)$, and $d_{\alpha N}(i,i+j)$ represent NOEs between $C_\alpha H(i)$ and NH(i+1, 2, and >2); $d_{NN}(i,i+1)$, $d_{NN}(i,i+2)$, $d_{NN}(i,i+3)$, and $d_{NN}(i,i+j)$ represent NOEs between NH(i) and NH(i, i+1, 2, 3, and >3); $d_{\beta N}(i,i+1)$ and $d_{\alpha\alpha}(i,i+j)$ represent NOEs between $C_\beta H(i)$ and NH(i,i+1) and between $C_\alpha H(i)$ and $C_\alpha H(i,i+j)$ protons, respectively. The symbol ○ represents the ϕ torsion angles which were obtained using direct measurement of the $^3J_{HN-H\alpha}$ scalar coupling constants from a single pulse "watergate" experiment.

protons from the proline ring were observed. The cysteines were first identified as AMX spin systems followed by the sequential assignment of the NOESY spectra. NOE peaks were observed between the Cβ−Cβ protons of Cys-6−Cys-16 and Cys-7−Cys-20, respectively. Sequence-specific resonance assignments were achieved using the standard methods established by Wüthrich and co-workers (*25*, *26*).

Structure Calculations. Interproton distance restraints were obtained from the NOESY spectra, with a NOESY buildup rate of 200 ms. Quantitative determination of cross-peak intensities was based on counting the exponentially spaced contour levels. The NOEs were subdivided corresponding to the following criteria: strong NOEs, 1.8 Å ≤ d ≤ 2.8 Å; medium NOEs, 1.8 Å ≤ d ≤ 3.5 Å; weak NOEs, 1.8 Å ≤ d ≤ 5 Å. The backbone dihedral angle constraints (five in total) for ϕ were obtained by measurement of the line width at half-height from 1D ^{1}H NMR spectrum following full NOESY NOE assignments. The $^3J_{\alpha NH}$ coupling constants were assumed to be related to the ϕ angles via the Karplus equation (*27*, *28*). For structure calculations these five backbone ϕ angles all have J couplings greater than 8 Hz and were restrained to −120 ± 30°. Interpretation of NOEs for side chain protons, which could not be assigned stereospecifically, was carried out by using pseudoatoms as reference points, and standard distance corrections were applied to these restraints (*29*).

Table 1: ^{1}H NMR Chemical Shifts, δ (ppm), Obtained for Ib-AMP1 in H_2O Solution at 30 °C and pH* 4.00

	chemical shifts, δ (ppm)[a]			
residue	NH	C_αH	C_βH	others
Glu-1	7.69	4.19	1.48, 2.23	C_γH 1.99, 2.24
Trp-2	8.18	4.70	3.24, 3.38	4H 7.38; 5H 6.88; 6H 7.148
Gly-3	8.23	3.72, 3.89		
Arg-4	7.92	4.44	1.58, 1.80	C_γH 1.51; C_δH 2.67, 2.74
Arg-5	4.73	1.78,	1.88	C_γH 1.70; C_δH 3.27; N_ϵH 7.23
Cys-6	9.15	4.07	2.00, 2.26	
Cys-7	8.90	4.86	2.78, 3.10	
Gly-8	7.45	3.55, 4.12		
Trp-9	9.14	4.67	3.07, 3.21	2H 7.44; 4H 7.65; 5H 7.18; 6H 7.26; 7H 7.52
Gly-10	8.71	3.23, 4.27		
Pro-11		4.38	1.958, 2.34	C_γH 2.08, 2.18; C_δH 3.49, 3.70
Gly-12	9.07	3.79, 3.93	1.958, 2.34	
Arg-13	7.39	4.12	1.79, 1.96	C_γH 1.58, 1.73; C_δH 3.25; N_ϵH 7.23
Arg-14	8.47	3.60	1.21, 1.30	C_γH 0.81, 1.20; C_δH 2.37, 2.64; N_ϵH 6.58
Tyr-15	7.49	4.93	2.99, 3.26	2,6H 6.93;3, 5H 6.83
Cys-16	9.17	3.79	1.69, 2.01	
Val-17	8.30	4.26	2.07	C_γH 0.61, 0.90
Arg-18	7.44	4.47	1.37, 1.49	C_γH 1.34, 1.54; C_δH 3.07, 3.17; N_ϵH 7.17
Trp-19	8.90	4.80	3.00, 3.26	2H 7.01; 4H 7.38; 5H 7.17; 6H 6.77; 7H 7.13
Cys-20	9.22	4.68	2.94, 3.20	

[a] Where no chemical shifts are given, these resonances were not observed or assigned.

Two separate sets of structure calculations were performed:

(1) The program DIANA (version 2.8) (*30*) was used to generate structures starting from all the NOEs observed, including the dihedral angle constraints. Ambiguities in the NOE assignments and satisfaction of the distance constraints were resolved in an iterative manner by comparison of the violation list obtained from the DIANA results to the NOEs assigned in the NOESY spectra. For this purpose 50 structures were generated in each of the iterative cycles with no disulfide restraints included. When all distance constraints were satisfied and assigned, two further calculations were performed, including disulfide distance constraints (2.00 Å < d_{S-S} < 2.02 Å) with the following disulfide connectivities: Cys-6−Cys-16, Cys-7−Cys-20 and Cys-6−Cys-20, Cys-7−Cys-16, respectively. This resolved any ambiguities over the assignment of the disulfide connectivities. The standard minimization protocol in DIANA was used, requiring 20 levels (L) for this 20-residue peptide. The weighting

Table 2: Summary of Restraints and Results of the Structure Calculations Obtained from X-PLOR

summary of $^1H-^1H$ restraints[a]	
total	104
sequential	33
medium range	59
long range	12
dihedral angle[b] ϕ	5
results	
backbone pairwise rmsd[c]	0.87 ± 0.27 Å
non-hydrogen atom pairwise	5.00 ± 1.16 Å
energies[d] (kcal·mol^{-1})	
$E_{overall}$	34.35 ± 2.05
E_{NOE}	2.82 ± 0.023
E_{cdih}	2.81 ± 0.21
E_{imp}	1.91 ± 0.24
E_{angle}	26.60 ± 0.54
E_{bonds}	1.67 ± 0.002
E_{vdW}	1.31 ± 0.41

[a] For medium range, restraints between residues whose sequence separation is ≤4 residues. For long range, restraints between residues whose sequence separation is >4 residues. [b] The number of restraints derived from $^3J_{HN-HA}$ > 8.0 Hz for which ϕ was set to −120 ± 30° for structure calcutations. [c] Pairwise rmsd calculated for residues 6−20. [d] Represents the structural statistics for 26 simulated anealing structures using X-PLOR. None of the structures exhibited violations greater than 0.2 Å or dihedral angle violations greater than 3°. The square-well NOE (E_{NOE}) using r^{-6} averaging, the restraint dihedral (E_{cdih}), torsional angles (E_{imp}), the angle (E_{angle}), the bond (E_{bonds}), and the quartic van der Waals repulsion energies (E_{vdW}) were calculated using force constants of 50 kcal·mol^{-1}·A^{-2}, 200 kcal·mol^{-1}·rad^{-2}, 500 kcal·mol^{-1}·rad^{-2}, 500 kcal·mol^{-1}·rad^{-2}, 1000 kcal·mol^{-1}·rad^{-2}, and 4 kcal·mol^{-1}·rad^{-4}, respectively. The van der Waals repulsion energy term was calculated using sphere radii set to 0.75 times that supplied with X-PLOR (parallalhdg.pro).

factors for the distance limits and the van der Waals constraints were set to unity and 0.2, respectively. However, in the final stage (L = 20) three minimization steps were carried out, increasing the van der Waals weighting factor from 0.2 to 0.6−2.0. For the final set, 250 structures were generated.

(2) Following the distance geometry calculations, the program X-PLOR (version 3.1+) (*31*) was used to search all conformational space, with the final distance constraints, dihedral constraints, and the disulfide connectivities determined in the DIANA calculations. The standard protocols, as reported in the X-PLOR manual, were used: initially 100 template coordinate sets with arbitrarily extended conformations with ideal geometry were generated. An *ab initio* simulated annealing protocol was followed with a starting temperature of 1000 K, allowing 15 000 steps in both high-temperature and cooling stages.

Structures produced from the *ab initio* simulated annealing were further refined using the *refine gentle* protocol with the initial temperature set at 300 K, with 20 000 cooling steps.

All structure calculations were performed on a Silicon Graphics Challenge server or on an Indy workstation.

RESULTS

Mass Spectroscopy. A single sharp peak of molecular mass 2463 Da was recorded and agrees with the expected mass of 2464.3 Da for this sequence (*15*). Determination of disulfide connectivities was not successful due to the sequential cysteines at positions 6 and 7 which could not be resolved by protease digest methods.

Circular Dichroism. CD results at various temperatures and pH values (panels a and b of Figure 2, respectively) show a large absorbance in the region of 190−195 nm. Compared to the standard spectra (*32*), the shape of this spectrum shows no evidence for α-helix or β-strand conformers but suggests that there may be some β−turns in the structure. There is almost no change in the CD spectrum from 19 to 90 °C, indicating little change in the secondary structure. pH titration studies showed little variation across a wide pH range (4−10). Due to the numerous aromatic residues, a broad CD spectrum in the aromatic region (data not shown) was obtained. Concentration studies reveal that the protein tends to precipitate at higher concentrations (>3 mM).

NMR Resonance Assignments. All NOE cross-peaks have been assigned. Very few medium- and long-range NOEs were observed. Furthermore, few NOEs are observed

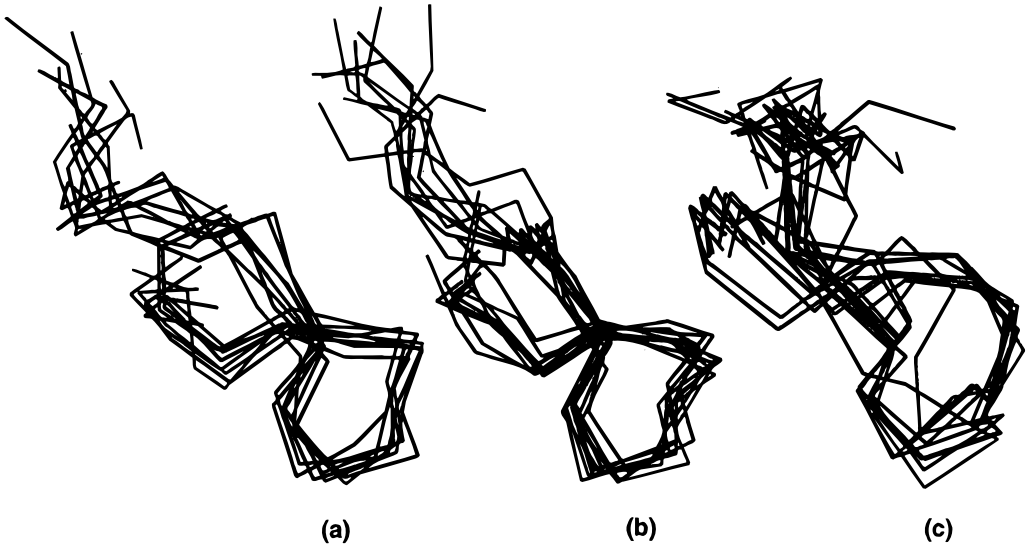

FIGURE 5: Superposition of the C_α trace for the top 10 structures obtained from DIANA for Ib-AMP1. Parts a, b, and c were obtained with no disulfide connectivities defined, with disulfide connectivities defined and as assigned from the NOESY NMR spectra, and with the alternate disulfide connectivities, respectively.

Table 3: Results of DIANA Runs for the Three Separate Structure Calculations for Ib-AMP1[a]

	structure set A	structure set B	structure set C
	no disulfide, connectivity	Cys-6−Cys-16, Cys-7−Cys-20	Cys-6−Cys-20, Cys-7−Cys-16
target function			
first structure	1.12	1.15	4.78
tenth structure	1.46	1.53	5.78
no. of consistent violations and violation type	none	none	7 HA Cys-6−HA Trp-19 HN Cys-7−HA Cys-20 HB* Cys-7−HB* Cys-20 HA* Gly-8−HN Trp-9 HB* Trp-19−HN Cys-20 angle ϕ Cys-7
mean rmsd	2.165	2.05	2.53
rmsd between structures with the lowest target functions with respect to the structure with no disulfide connectivity		1.72	3.63

[a] The table shows the target functions, list of consistent NOE violations, mean rmsd comparison for the top 10 structures, and comparison of rmsd for structures with the lowest target function with respect to the structure with the lowest target function with the disulfide connectivity, C6−C16, C7−C20 and C6−C20, C7−C16, respectively. The target functions given are for the first and the tenth structures.

FIGURE 6: Superposition of the backbone for 26 solution structures of Ib-AMP1.

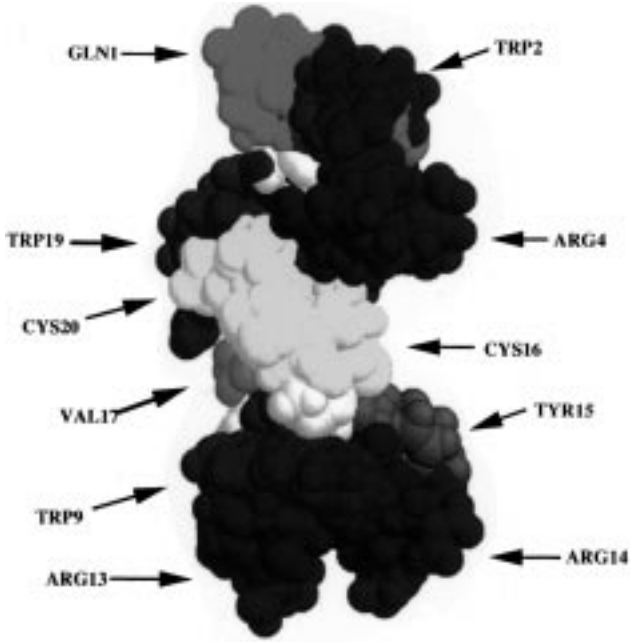

FIGURE 7: Space-filling models of the backbone and heavy atom conformations for the five representative structures of Ib-AMP1 [as obtained from NMRCLUST (*34*) with the related subfamilies being superimposed].

between the side chains and the backbone. Figure 3 shows the fingerprint region of the NOESY spectrum in H_2O of Ib-AMP1. Experiments performed in D_2O showed no slowly exchanging NH's, eliminating main chain hydrogen bonds and further suggesting that no helix or β-sheet structures were present. NOESY NMR experiments carried out at 10 °C revealed very little difference to the NMR spectra obtained at 30 °C. A summary of the observed sequential and interresidue NOE connectivities is shown in Figure 4. In addition, NOEs between the C_β protons of, first, Cys-6 and Cys-16 and, second, Cys-7 and Cys-20 are also observed. Strong NOEs were observed between gly10 C_α protons to the C_δ protons of the proline ring. These NOEs suggest that the peptide bond between glycine and proline adopts a trans conformation. Table 1 lists the resonance assignments, and Table 2 gives a summary of the input restraints used for the structural calculations for Ib-AMP1.

Figure 5 and Table 3 show the results of DIANA calculations for Ib-AMP1. Figures 5 compares the superpositions of the C_α traces for the top 10 structures obtained from the three runs using DIANA. The structures were derived with no disulfide constraints applied (Figure 5a); those in Figure 5b include disulfide connectivities defined and as assigned from the NOESY NMR spectra (Cys-6−Cys-16, Cys-7−Cys-20), and Figure 5c corresponds to structures with the alternative disulfide connectivities (Cys-6−Cys-20 and Cys-7−Cys-20). For each calculation, Table 3 shows the target functions, a list of consistent NOE violations, and the mean C_α rmsd between these structures for the best 10 structures. Comparison of the three structures with the lowest target function for each calculation is also presented by the rmsd values. The target functions given are for the first and the tenth structure. Comparison of the three ensembles in Figure 5b clearly shows that the ensemble derived with restraints between Cys-6−Cys-16 and Cys-7−Cys-20 is very similar to that derived with no such restrictions (Figure 5a). In contrast, the ensemble with the restraints between Cys-6−Cys-20 and Cys-7−Cys-16 is very different and also a poorer solution with more violations. We can

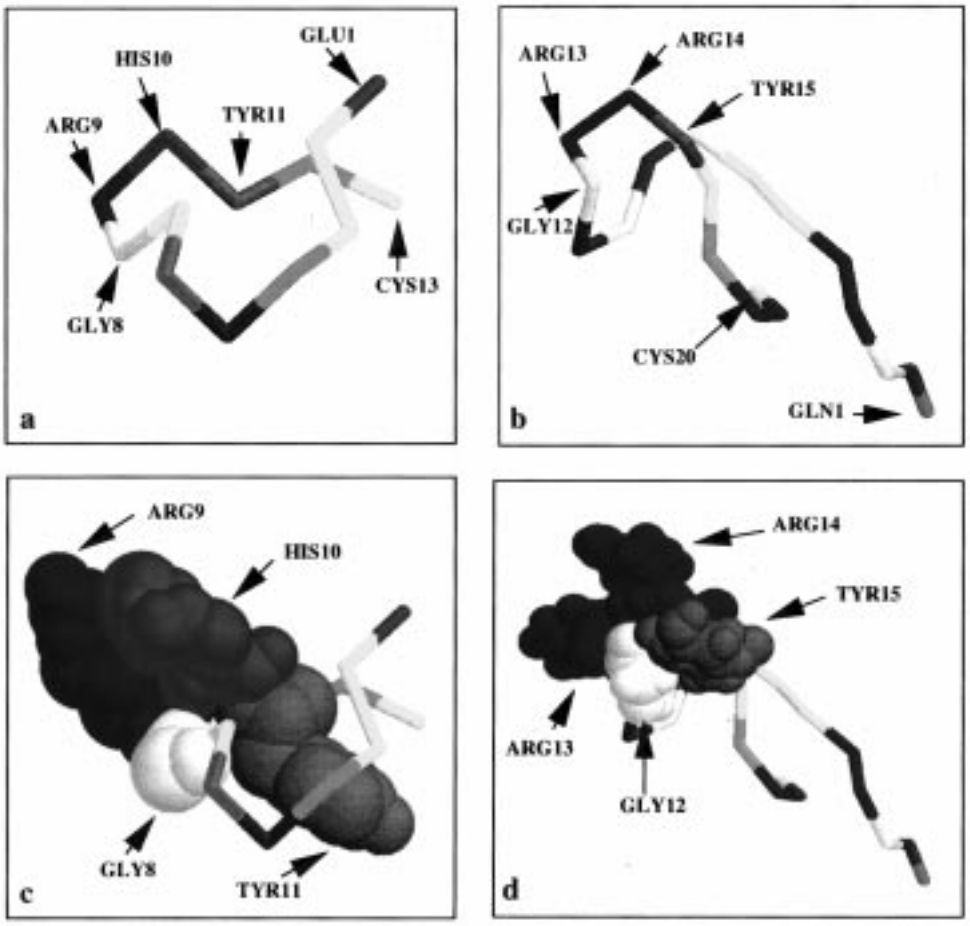

FIGURE 8: Panels a and b show the backbone structures of the α-conotoxin G1 and *I. balsamina* Ib-AMP1. Panels c and d show space-filling models of the conformation adopted by the side chains for the conserved residues GRR/HY.

conclude that the long-range NOE restraints and the local $C_\beta-C_\beta$ proton restraints both support the Cys-6−Cys-16, Cys-7−Cys-20 connectivity.

During the initial iterative structure calculations in X-PLOR, two families of structures were generated, one being the mirror fold of the other. However, upon structural refinements, only one family emerged which satisfied all the data. No such mirror image folds were observed during structure calculations using DIANA. These models were required to have no NOE violations greater than 0.2 Å and no dihedral angle violations greater than 5° and to exhibit the lowest energies as obtained from X-PLOR structure calculations and analyzed by Aqua and PROCHECK NMR (*33*). Figure 6 shows a superposition of the backbone for the 26 structures with the lowest overall energies out of the 100 structures generated. The NOE data and the results of the structure calculations suggest that although the backbone is well defined, the N-terminus and the side chains are very floppy.

Analysis of the 26 models by superimposing the backbone for residues 6−20 and using the program NMRCLUST (*34*) gave five sets of conformationally related subfamilies with differences in their rmsd (data not shown). Figure 7 shows space-filling models of the backbone and heavy atom conformation for the five representative structures from the related subfamilies being superimposed.

Structural analysis of the ensemble using the program PROMOTIF (*35*) suggests that residues 9−12 (WGPS), residues 10−13 (GPGR), and residues 12−15 (GRRY) generally form β-turns of types IV, I and IV, respectively. Table 2 also lists the structural statistics obtained from the X-PLOR calculations.

DISCUSSION

Although this is a low-resolution structure, it is clear that this small peptide has a well-resolved structured core which is sufficiently defined to suggest that it may be involved in specific intermolecular interactions. Unlike many other small antimicrobial peptides, it does not form an amphipathic helix and so is unlikely to function by nonspecific membrane disruption. In contrast, the peptide may well interact with a specific receptor. Superposition of the backbone for the structures generated revealed the N-terminus (residue 1−5) and the side chains to be floppy while the backbone for residues 6−20 is relatively well defined (rmsd for the backbone is 0.92 Å), forming a distinctive loop structure. Two hydrophilic patches are observed at opposite ends and at opposite sides of the models, consisting of residues Arg-4, Arg-5, and Arg-18 and residues Arg-13 and Arg-14, respectively. Sandwiched in between the two hydrophilic patches is a large hydrophobic patch consisting of residues Trp-9, Val-17, and Trp-19 and the cysteines. This patch is on the same face of the protein as the GPGRR Arg-13 and Arg-14 hydrophilic patch (Figure 7). Interestingly, structural calculations using no disulfide restraints gave conformations similar to those obtained with disulfide restraints between

Cys-6−Cys-16 and Cys-7−Cys-20. Replacement of the cysteines by α-amino-butyric acid shows that the non-disulfide-linked peptide adopts a random coil conformation (Fant, personal communication), confirming that the loop conformation adopted by the peptide is due to the disulfide restraints.

A sequence search of the protein sequence data-bases for Ib-AMP1 failed to identify any protein/peptide with statistically significant homology. However, the most closely related peptides were found to be the α-conotoxins isolated from marine snails; see Figure 1 (*36*−*46*). Although the disulfide connectivities are similar with a +2,+2 type connectivity in both families of peptides, the alignment is otherwise weak. Sequence comparison of Ib-AMP1 with α-conotoxins GI, GIA, and GII shows several interesting features: Ib-AMP1 has a longer N-terminus (residues 1−5), and the lengths of the inter-cysteine loops have changed. Interestingly, the sequence GRR/HY is observed in both families but in different loops.

Recently two crystal structures of the α-conotoxins G1 and PnIA have been determined (*47*, *48*). Structural comparison of Ib-AMP1 with these two α-conotoxins shows that the two folds are not similar. In the crystal structure of the α-conotoxin G1, Asn-4−Cys-7 and Gly-8−Tyr-11 form a short 3_{10} helix and type I β-turn, respectively. The α-conotoxins such as G1 are known to cause muscular paralysis by antagonising acetylcholine binding to the postsynaptic acetylcholine receptor at the neuromuscular junction (*36*−*46*, *49*). By analogy with D-tubocurarine (*50*) and snake venoms such as the α-bungarotoxin and erabutoxin (*51*−*54*) which block neurotransmission, the active "site" on the α-conotoxin is thought to comprise of quaternary cationic centers Glu-1 and Arg-9 and lipophilic centers His-10 and Tyr-11. No similar active center was found in Ib-AMP1. Structural comparison of Ib-AMP1 and the α-conotoxin G1 (*47*, *55*, *56*) for the conserved GRR/HY sequence shows that although both are involved in a turn, they have different loop conformations (Figure 8). Interestingly, in the α-bungarotoxin assay using an insect receptor preparation to see whether Ib-AMP1 might bind to the acetylcholine receptor, no displacement of α-bungarotoxin was observed even when Ib-AMP1 was added at 1000 times the concentrations of labeled toxin. There are major differences in the overall charges and the distribution of polar and nonpolar residues between α-conotoxin and Ib-AMP1. This positioning of charges in the different loops may be of functional importance as has been shown for the α-conotoxins.

From the experimental data, the variant Ib-AMP4 has a higher antifungal activity than Ib-AMP1 particularly in high ionic strength media (*15*), despite exhibiting only a single amino acid change of Val-17 to arginine. From homology modeling studies (data not shown) this extra positive charge extends the hydrophilic patch formed by residues Arg-4, Arg-5, and Arg-18. Further mutagenesis and binding studies will be needed to unravel the mode of action of this potent antifungal peptide.

ACKNOWLEDGMENT

We thank Judith Blythe (Zeneca Agrochemicals) for carrying out the acetylcholine binding assay and the MRC Biomedical NMR Centre, National Institute for Medical Research, Mill Hill, London, ULIRS NMR (Queen Mary and Westfield College, University of London), and the Ludwig Institute for Cancer Research for the provision of the NMR facilities and the technical staff for their help. We also thank the technical staff, in particular Mrs. B. Banfield at the National Chiroptical Spectroscopy Centre (EPSRC), Department of Chemistry, Birkbeck College, University of London, for acquiring the CD spectra and for the provision of CD facilities.

REFERENCES

1. Schumbaum, A., Mauch, F., Vogeli, U., and Boller, T. (1986) *Nature 324*, 365−367.
2. Broekaert, W. F., Van Parjis, J., Allen, A. K., and Peumans, W. J. (1988) *Physiol. Mol. Plant Pathol. 33*, 319−331.
3. Broekaert, W. F., Van Parjis, J., Leyns, F., Joos, H., and Peumans, W. J. (1989) *Science 245*, 1100−1102.
4. Roberts, W. K., and Selitrennikoff, C. P. (1986) *Biochim. Biophys. Acta 880*, 161−170.
5. Mauch, F., Mauch-Mani, B., and Boller, T. (1988) *Plant Physiol. 88*, 936−942.
6. Manners, D. J., and Marshall, J. J. (1973) *Phytochemistry 12*, 547−553.
7. Bernhard, W. R., and Somerville, C. R. (1989) *Arch. Biochem. Biophys. 269*, 695−697.
8. Van Parjis, J., Broekaert, W. F., Goldstein, I. J., and Peumans, W. J. (1991) *Planta 183*, 258−264.
9. Moreno, J., and Chrispeels, M. J. (1989) *Proc. Natl. Acad. Sci. U.S.A. 86*, 7885−7889.
10. Bohlmann, H., Clausen, S., Behnkn, S., Giese, H., Hiller, C., Reimann-Philipp, U., Schrader, G., Barkholt, V., and Apel, K. (1988) *EMBO J. 7*, 1559−1565.
11. Bohlmann, H., and Apel, K. (1991) *Annu. Rev. Plant Physiol. Plant Mol. Biol. 42*, 227−240.
12. Fernandez de Caleya, R., Gonzales-Pascual, B., Garcia-Olmedo, F., and Carbonero, P. (1972) *Appl. Microbiol. 23*, 989−1000.
13. Broekaert, W. F., Cammue, B. P. A., De Bolle, M., Thevissen, K., De Samblank, G. W., and Osborn, R. (1997) *Crit. Rev. Plant Sci. 16*, 297−323.
14. Osborn, R. W., De Samblank, G. W., Thevissen, K., Goderis, I., Torrekens, S., Leuven, F. V., Attenborough, S., Rees, S. B., and Broekaert, W. F. (1995) *FEBS Lett. 368*, 257−262.
15. Tailor, R. H., Acland, D. P., Attenborough, S., Cammue, B. P. A., Evans, I. J., Osborn, R. W., Ray, J. A., Rees, S. B., and Broekaert, W. F. (1997) *J. Biol. Chem. 272*, 24480−24487.
16. Rance, M., Sorensen, O. W., Bodenhausen, G., Wagner, G., Ernst, R. R., and Wüthrich. K. (1983) *Biochem. Biophys. Res. Commun. 117*, 479−485.
17. Braunschweiler, L., and Ernst, R. R. (1983) *J. Magn. Reson. 53*, 521−528.
18. Davis, D. G., and Bax, A. (1985) *J. Am. Chem. Soc. 107*, 2820−2821.
19. Jeener, J., Meier, B. H., Bachmann, P., and Ernst, R. R. (1979) *J. Chem. Phys. 71*, 4546−4553.
20. Macura, S., Huong, Y., Suter, D., and Ernst, R. R. (1981) *J. Magn. Reson. 43*, 259−281.
21. Bax, A., and Davis, D. G. (1985) *J. Magn. Reson. 65*, 355−360.
22. Piotto, M., Saudek, V., and Sklenar, V. (1992) *J. Biomol. NMR. 2*, 661−665.
23. States, D. J., Haberkorn, R. A., and Ruben, D. J. (1982) *J. Magn. Reson. 48*, 286−292.
24. *VNMR, Version 4.3* (1989−1993) Varian Associates Inc., Nuclear Magnetic Instruments, 3120 Hansen Way, Palo Alto, CA 94304-1030.
25. Wagner, G., and Wüthrich, K. (1982) *J. Mol. Biol. 155*, 347−366.
26. Wüthrich, K. (1986) *NMR of Proteins and Nucleic Acids*, John Wiley and Sons, Inc., New York.
27. Karplus, M. (1959) *J. Chem. Phys. 30*, 11−14.

28. Pardi, A., Billeter, M., and Wüthrich, K. (1984) *J. Mol. Biol. 180*, 741−751.
29. Wüthrich, K., Billeter, M., and Braun, W. (1983) *J. Mol. Biol. 169*, 949−961.
30. Guntert, P., Braun, W., and Wüthrich, K. (1991) *J. Mol. Biol. 217*, 517−530.
31. Brunger, A. T. (1992) *X-PLOR Version 3.1*, Yale University, New Haven, CT.
32. Drake, A. F. (1994) in *Methods in Molecular Biology, Vol. 22, Microscopy, optical spectroscopy and macroscopic technology* (Jones, C., Mulloy, B., and Thomas, A. H., Eds.) Humana Press Inc., Totowa, NJ.
33. Laskowski, R. A., Rullmann, J. A. C., MacArthur, Kaptein, R., and Thornton, J. M. (1996) *J. Biomol. NMR 8*, 477−496.
34. Kelley, L. A., Gardner, S. P., and Sutcliffe, M. J. (1996) *Protein Eng. 9*, 1063−1065.
35. Hutchinson, E. G., and Thornton, J. M. (1996) *Protein Sci. 5*, 212−220.
36. Gray, W. R., Lugue, F. A., Olivera, B. M., Barret, J., and Cruz, L. J. (1981) *J. Biol. Chem. 256*, 4734−4740.
37. Gray, W. R., Lugue, F. A., Galyean, R., Atherton, E., Sheppard, R. C., Stone, B. L., Reyes, A., Alford, J., McIntosh, M., Olivera, B. M., Cruz, L. J., and River, J. (1984) *Biochemistry 23*, 2796−2802.
38. Myers, R. A., Zafaralla, G. C., Gray, W. R., Abbot, J., Cruz, L. J., and Olivera, B. M. (1991) *Biochemistry 30*, 9370−9377.
39. Zafaralla, G. C., Ramilo, C. A., Gray, W. R., Karlstrom, R., Olivera, B. M., and Cruz, L. J. (1988) *Biochemistry 27*, 7102−7105.
40. Ramilo, C. A., Zafaralla, G. C., Nadasdi, L., Hammerland, L. G., Yoshikami, D., Gray, W. R., Kristipati, R., Ramachandran, J., Miljanich, G., Olivera, B. M., and Cruz, L. J. (1992) *Biochemistry 31*, 9919−9926.
41. McIntosh, J. M., Cruz, L. J., Hunkpillar, M. W., Gray, W. R., and Olivera, B. M. (1982) *Arch. Biochem. Biophys. 218*, 329−334.
42. McIntosh, J. M., Yoshikami, D., Mahe, E., Nielsen, D. B., Rivier, J. E., Gray., W. R., and Olivera, B. M. (1994) *J. Biol. Chem. 269*, 16733−16739.
43. McIntosh, J. M., Hasson, A., Spira, M. E., Gray, W. R., Li, W. Q., Marsh, M., Hillyard, D. R., and Olivera, B. M. (1995) *J. Biol. Chem. 270*, 16796−16802.
44. Cartier, G. E., Yoshikami, D., Gray, W. R., Luo, S., Olivera, B. M. and McIntosh, J. M. (1996) J. *Biol. Chem. 271*, 7522−7528.
45. Fainzilber, M., Hasson, A., Oren, R., Burlingame, A. L., Gordon, D., Spira, M. E., and Zlotkin, E. (1994) *Biochemistry 33*, 9523−9529.
46. Martinez, J. S., Olivera, B. M., Gray, W. R., Craig, A. G., Groebe, D. R., Abramson, S. N., and McIntosh, J. M. (1995) *Biochemistry 34*, 14519−14526.
47. Guddat, L. W., Martin, J. A., Shan, L., Edmundson, A. B., and Gray, W. R. (1996) *Biochemistry 35*, 11329−11335.
48. Hu, S.-H., Gehrmann, J., Guddat, L. W., Alewood, P. F., Craik, D. J., and Martin, J. L. (1996) *Structure*, 417−423.
49. Hucho, F., Tsetlin, V. I., and Machold, J. (1996) *Eur. J. Biochem. 239*, 539−557.
50. Peterson, S. E., and Cohen, J. B. (1990) *Proc. Natl., Acad. Sci. U.S.A. 87*, 2785−2789.
51. Basus, V. J., Song, G. A., and Hawrot, E. (1993) *Biochemistry 32*, 12290−12298.
52. Pillet, L., Tremeau, 0., Ducancel, F., Drevet, P., Zinn-Justin, S., Pinkasfeld, S., Beulain, J. C., and Menez, A. (1993) *J. Biol. Chem. 268*, 909−916.
53. Hatanaka, H., Oka, M., Kohda, D., Tate, S., Suda, A., Tamiya, N., and Inagaki, F. (1994) *J. Mol. Biol. 240*, 155−160.
54. Tremeau, O., Lemaire, C., Drevet, P., Pinksfield, S., Duncancel, F., Boulain, J. C., and Menez, M. (1995) *J. Biol. Chem. 270*, 9362−9369.
55. Pardi, A., Galdes, J. F., and Maniconte, D. (1989) *Biochemistry 28*, 5494−5501.
56. Kobayshi, Y., Ohkubo, T., Yoshimasa, K., Nishiuchi, Y., Sakakibara, S., Bruan, W., and Go, N. (1989) *Biochemistry 28*, 4853−4860.

BI971747D